frontiers in Chemistry

ORIGINAL RESEARCH
published: 07 October 2021
doi: 10.3389/fchem.2021.743637

2D/3D Copper-Based Metal-Organic Frameworks for Electrochemical Detection of Hydrogen Peroxide

Xiangjian Guo[1,2], Chuyan Lin[1], Minjun Zhang[1], Xuewei Duan[1], Xiangru Dong[2], Duanping Sun[2], Jianbin Pan[3]* and Tianhui You[1]**

[1]School of Nursing, Guangdong Provincial Key Laboratory of Pharmaceutical Bioactive Substances, Guangdong Pharmaceutical University, Guangzhou, China, [2]Center for Drug Research and Development, Guangdong Provincial Key Laboratory of Pharmaceutical Bioactive Substances, Guangdong Pharmaceutical University, Guangzhou, China, [3]State Key Laboratory of Analytical Chemistry for Life Science, School of Chemistry and Chemical Engineering, Nanjing University, Nanjing, China

Metal-organic frameworks (MOFs) have been extensively used as modified materials of electrochemical sensors in the food industry and agricultural system. In this work, two kinds of copper-based MOFs (Cu-MOFs) with a two dimensional (2D) sheet-like structure and three dimensional (3D) octahedral structure for H_2O_2 detection were synthesized and compared. The synthesized 2D and 3D Cu-MOFs were modified on the glassy carbon electrode to fabricate electrochemical sensors, respectively. The sensor with 3D Cu-MOF modification (HKUST-1/GCE) presented better electrocatalytic performance than the 2D Cu-MOF modified sensor in H_2O_2 reduction. Under optimal conditions, the prepared sensor displayed two wide linear ranges of 2 μM–3 mM and 3–25 mM and a low detection limit of 0.68 μM. In addition, the 3D Cu-MOF sensor exhibited good selectivity and stability. Furthermore, the prepared HKUST-1/GCE was used for the detection of H_2O_2 in milk samples with a high recovery rate, indicating great potential and applicability for the detection of substances in food samples. This work provides a convenient, practical, and low-cost route for analysis and extends the application range of MOFs in the food industry, agricultural and environmental systems, and even in the medical field.

Keywords: copper-based metal-organic frameworks, electrochemical sensor, hydrogen peroxide, dairy products, detection

OPEN ACCESS

Edited by:
Chunsheng Wu,
Xi'an Jiaotong University, China

Reviewed by:
Thirumurugan Arun,
Universidad de Atacama, Chile
Zhi-Gang Gu,
Fujian Institute of Research on the Structure of Matter (CAS), China

****Correspondence:***
Duanping Sun
sundp@gdpu.edu.cn
Jianbin Pan
jbpan@nju.edu.cn
Tianhui You
youth888cn@aliyun.com

Specialty section:
This article was submitted to Nanoscience, a section of the journal Frontiers in Chemistry

Received: *19 July 2021*
Accepted: *03 September 2021*
Published: *07 October 2021*

Citation:
Guo X, Lin C, Zhang M, Duan X, Dong X, Sun D, Pan J and You T (2021) 2D/3D Copper-Based Metal-Organic Frameworks for Electrochemical Detection of Hydrogen Peroxide. Front. Chem. 9:743637. doi: 10.3389/fchem.2021.743637

INTRODUCTION

Hydrogen peroxide (H_2O_2) is widely used in the food industry, medical field, textile industry, and paper industry (Zhang and Chen, 2017). Generally, H_2O_2 works as an antibacterial agent, bleaching agent (Kang et al., 2010), stabilizer, and preservative (Singh and Gandhi, 2015) in dairy products. Based on the laws and the rules, manufacturers are not allowed to add H_2O_2 in excess. H_2O_2 in abnormal level will damage human health, resulting in Alzheimer's disease, cancer, and cardiovascular diseases (Upadhyay et al., 2014; Akyilmaz et al., 2017; Nascimento et al., 2017). Therefore, it is important to detect H_2O_2 in dairy products to protect public health and normalize the production with some benefits (Tang et al., 2010; Karimi et al., 2018). Nowadays, many analytical methods have been applied for the detection of H_2O_2, such as high-performance liquid chromatography (Ivanova et al., 2019), spectrophotometry (Li et al., 2017a), chemiluminescence (Li et al., 2017b), colorimetry (Dominguez-Henao et al., 2018; Yao et al., 2020), fluorescence (Pundir et al., 2018), and electrochemistry. Nevertheless, some of them are time consuming, of high

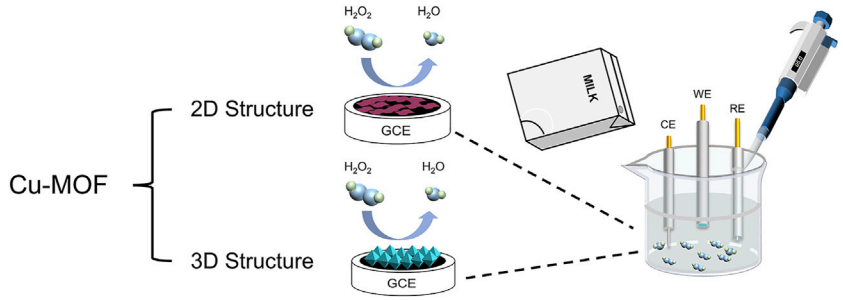

SCHEME 1 | Schematic illustration of Cu-MOFs detecting H_2O_2 from the milk sample using the electrochemical method.

consumption, and need advanced instruments or experienced and professional staff (Sun et al., 2016). Among them, electrochemistry has drawn attention due to rapid response (Ammam and Fransaer, 2010), high selectivity (Conzuelo et al., 2010), simple operation (Stankovic et al., 2020), and real-time detection. Electrochemical methods can be used as an alternative to other techniques as a result of their limited drawbacks. Dong et al. designed $ZnFe_2O_4$/SWCNTs/GCE as a new sensor for the electrochemical detection of pesticides in apples, tomatoes, leeks, and water samples (Dong et al., 2017). Vinitha Mariyappan et al. synthesized Gd_2S_3/RGO hybrid composites and modified on the surface of the glassy carbon electrode (GCE) to serve as an electrochemical platform for the detection of carbofuran in potatoes and river water samples (Mariyappan et al., 2021). Therefore, the electrochemical method is a promising strategy for the detection of H_2O_2 in dairy products.

A metal-organic framework (MOF) is a crystalline porous material constructed by coordination of metal ions or clusters with polytopic organic ligands (Furukawa et al., 2013). They possess many promising features like tunable structures, active sites, rapid electron transmission, and high surface area (Lee et al., 2009; Gu et al., 2014). MOFs have been extensively used in electrochemical applications (Chen et al., 2020; Lu et al., 2020; Wei et al., 2020), gas storages (Hinks et al., 2010; Zhang et al., 2020), and biomedical fields like wound healing (Fu et al., 2020; Chen et al., 2021), enhanced cancer therapy (Luo et al., 2019), imaging (Lu et al., 2018), antibacterial agents (Qi et al., 2020), cell detection (Shi et al., 2021), and drug delivery (Simon-Yarza et al., 2018) because of excellent physical and chemical properties. In addition, MOFs with catalytic activity have become an ideal modified material of electrochemical sensors for detection in real samples (Guo et al., 2020; He et al., 2020; Liu et al., 2020; Zhang et al., 2021). For example, Luan et al. prepared iron-based MOFs with modification (NMOF-Pt-sDNA) to detect kanamycin in milk samples (Luan et al., 2017). Zeng et al. modified copper-based metal-organic frameworks (Cu-MOFs) as a template to construct a nonenzyme electrochemical unit for H_2O_2 sensing in milk and human serum samples (Zeng et al., 2019). However, MOFs with different structures present a unique electrocatalytic property. Morphology and structure strongly affect their chemical and physical properties (Sun et al., 2020). Two-dimensional metal-organic frameworks (2D MOFs) with ultrathin thickness morphology and an ultrahigh surface area possess many accessible active sites on their surface. Thus, the catalytic and sensing applications could benefit from the inherent properties of 2D MOFs (Zhao et al., 2015; Zhao et al., 2018). Three-dimensional metal-organic frameworks (3D MOFs) with diverse morphology present outstanding chemical and physical properties in detection (Xue et al., 2019). It is meaningful to explore different structures of MOFs based on the same metal ions and study their electrochemical catalysis and other properties to investigate the mechanism.

As a typical series of MOFs, Cu-MOFs have been reported for many years. A classic version of 2D Cu-MOFs named Cu–TCPP has been successfully developed and applied in optoelectronic materials, catalysis, and sensing (Lu et al., 2016; Wang et al., 2016). Cu–TCPP has a large specific surface area, tunable pore size, 2D planar structure, and perfect nanostructure. Cu-TCPP is composed of Cu^{2+} as metal ions and tetrakis (4-carboxyphenyl) porphyrin (TCPP) as organic ligands (Dong et al., 2020). Porphyrin is a member of heterocyclic compounds with a conjugated structure. On the other hand, porphyrins are one of the substances with peroxide mimicking enzyme activity (Ma and Zheng, 2020). The surfactant, such as polyvinylpyrrolidone (PVP), plays a significant role in 2D MOF synthesis. On the one hand, the surfactant prevents the MOF layers from stacking in the vertical direction which is contributed to form ultrathin MOF nanosheets. On the other hand, PVP would maintain the as-synthesized MOF nanosheets in stabilization, preventing their aggregation (Zhao et al., 2018). According to previous reports (Bai et al., 2019; Ma et al., 2020), Cu-TCPP has been applied for the detection of H_2O_2 in real samples, showing the potential of fabricating electrochemical sensors to detect H_2O_2. One of the most representative Cu-MOFs with a 3D structure named HKUST-1 or MOF-199 was first reported and synthesized by the Hong Kong University of Science and Technology in 1999 (Chui et al., 1999). The main structural characterization of HKUST-1 is a copper dimer with a copper–copper distance of 0.263 nm. The material is composed of twelve oxygen atoms, obtained from the carboxylate groups of the four 1, 3, 5-benzenetricarboxylate (BTC) ligands, which are bound to the four coordination sites of each of the three Cu^{2+} ions. The presented paddle-wheel units form a face-centered crystal

lattice with Fm-3m symmetry which possesses a three-dimensional porous network with a bimodal pore size distribution (Hartmann et al., 2008; Kim et al., 2012; Loera-Serna et al., 2012). It had an amount of open coordination sites, which was beneficial for detection (Li et al., 2018a). This kind of classic MOFs has been widely used in gas storage, biomedical field, and substance detection (Azad et al., 2016; Tan et al., 2017). However, there are little reports of pristine HKUST-1 as modified materials to construct an electrochemical sensor for the detection of H_2O_2 (Zhang et al., 2013; Yang et al., 2015). We are interested in investigating the comparison of 2D Cu-MOF (Cu-TCPP) and 3D Cu-MOF (HKUST-1) in H_2O_2 sensing.

In this study, two kinds of different structures of Cu-MOFs were synthesized successfully. As shown in **Scheme 1**, the 2D Cu-MOF and 3D Cu-MOF were coated on the surface of GCE to construct electrochemical sensors, respectively. The HKUST-1/GCE displayed a better catalytic ability and electrochemical performance than Cu-TCPP/GCE in H_2O_2 reduction because of the three-dimensional structure and better conductivity. Besides, 3D Cu-MOF/GCE (HKUST-1/GCE) had two wide linear ranges of 2 μM–3 mM and 3–25 mM, and the limit of detection (LOD) was 0.68 μM with high sensitivity and selectivity. Based on these satisfactory results, the HKUST-1/GCE was successfully used for detecting H_2O_2 in milk samples. These results indicated the influences of structures and morphology of MOFs in electrochemical catalysis and made a great difference in the detection of substances. It pointed out the significance of investigating the morphology of MOFs for further exploring and studying the mechanism.

METHODS AND MATERIALS

Materials and Reagents

Copper nitrate hydrate [Cu $(NO_3)_2{\cdot}xH_2O$], trimesic acid [$C_6H_3(CO_2H)_3$], sodium sulfate anhydrous (Na_2SO_4), citric acid monohydrate ($C_6H_8O_7{\cdot}H_2O$), and ascorbic acid ($C_6H_8O_6$) were obtained from Aladdin Reagent Co., Ltd. (Shanghai, China). Polyvinylpyrrolidone [PVP, molecular weight (Mw) = 40,000] was obtained from Sigma–Aldrich Co., Ltd. Tetrakis (4-carboxyphenyl) porphyrinabsolute (TCPP) was obtained from Tokyo Chemical Industry Co., Ltd. Sodium chloride (NaCl), disodium hydrogen phosphate (Na_2HPO_4), potassium chloride (KCl), potassium dihydrogen phosphate (KH_2PO_4), potassium ferricyanide [$K_3Fe(CN)_6$], and potassium ferrocyanide trihydrate [$K_4Fe(CN)_6{\cdot}3H_2O$] were obtained from Sinopharm Chemical Reagent Co., Ltd. (Shanghai, China). Ethanol absolute (EtOH) and N, N-dimethylformamide (DMF) were bought from Tianjin Damao Chemical Reagent Co., Ltd. Nafion (5%) was brought from Alfa Aesar Co., Ltd. Hydrogen peroxide (H_2O_2) and methanol (CH_4O) were purchased from Guangzhou Chemical Reagent Co., Ltd. (Guangzhou, China). The phosphate buffered saline (PBS) (pH 7.2, 0.1 M) was prepared by mixing with 11.36 g Na_2HPO_4, 2.72 g KH_2PO_4, 0.20 g KCl, and 8.00 g NaCl into 1,000 ml ultrapure water. Ultrapure water (18.2 MΩ; Millipore Co., United States) was used to prepare all solutions. All solutions were stored at room temperature at 25 ± 2°C for further use. All reagents are of analytical grade without further purification.

Apparatus and Instrumentation

Scanning electron microscopy (SEM) images were photographed by a scanning electron micrograph (SEM, Hitachi Regulus 8230, Japan). Transmission electron microscopy (TEM) images were taken by a transmission electron microscope (JEM 1400, Japan). Fourier transform infrared (FT-IR) spectra were conducted on a Fourier transformation infrared spectrometer (IR, EQUINOX 55, Germany). X-ray powder diffraction (XRD) patterns were recorded on a PANalytical instrument (Empyrean, Netherlands) to examine the crystal phase of the samples. The surface composition and valence states were studied by X-ray photoelectron spectra (XPS, Nexsa, Thermo Fisher Scientific, United States). All electrochemical experiments were studied by a CHI 660E electrochemical workstation (Shanghai CH Instruments Co., China). The traditional three-electrode system was employed in this research. The bare or modified glassy carbon electrodes, platinum electrode, and saturated Ag/AgCl electrode were served as working electrodes, counter electrodes, and reference electrodes, respectively.

Synthesis of 2D Structure Cu-MOF

The synthesis process was based on a previous report (Ma and Zheng, 2020). First, 25 mg of Cu $(NO_3)_2{\cdot}xH_2O$ and 100 mg PVP were dissolved in 60 ml solution containing DMF and Ethanol absolute (V: V = 3:1) under stirring condition. Second, 60 mg of TCPP was added to the above solution and further ultrasonicated. Finally, the solution was poured into a Teflon autoclave heating for 4 h using the solvothermal method at 80°C. The red product was centrifuged, washed, dried, and stored at room temperature. The red product was named Cu-TCPP or 2D Cu-MOF.

Synthesis of 3D Structure Cu-MOF

The synthesis process was based on the preceding article (Wu et al., 2013). First, 1.82 g copper nitrate (Cu $(NO_3)_2{\cdot}xH_2O$) and 0.875 g trimesic acid ($C_6H_3(COOH)_3$) were dissolved in 50 ml absolute methanol under ultrasonication to get blue and transparent solutions, respectively. Second, the copper nitrate solution was added to the trimesic acid solution. Third, the mixture solution was kept at room temperature for 2 h until 3D Cu-MOF precipitation was finished. The blue product was centrifuged and washed with methanol two times. Lastly, the blue product named HKUST-1or 3D Cu-MOF was dried in vacuum condition for use.

Preparation of the Cu-MOF-Modified Electrode

Prior to modification, the bare GCE was polished with 0.05 mm Al_2O_3 powder and rinsed with deionized water and ethanol under ultrasonication for 2 min to get a mirror-like state. The mirror-like GCE was dried in nitrogen stream for use. 1 mg of 2D Cu-MOF or 3D Cu-MOF was dispersed in the solution containing ultrapure water and 5% Nafion solution (V: V = 2:0.004). 6 μL of

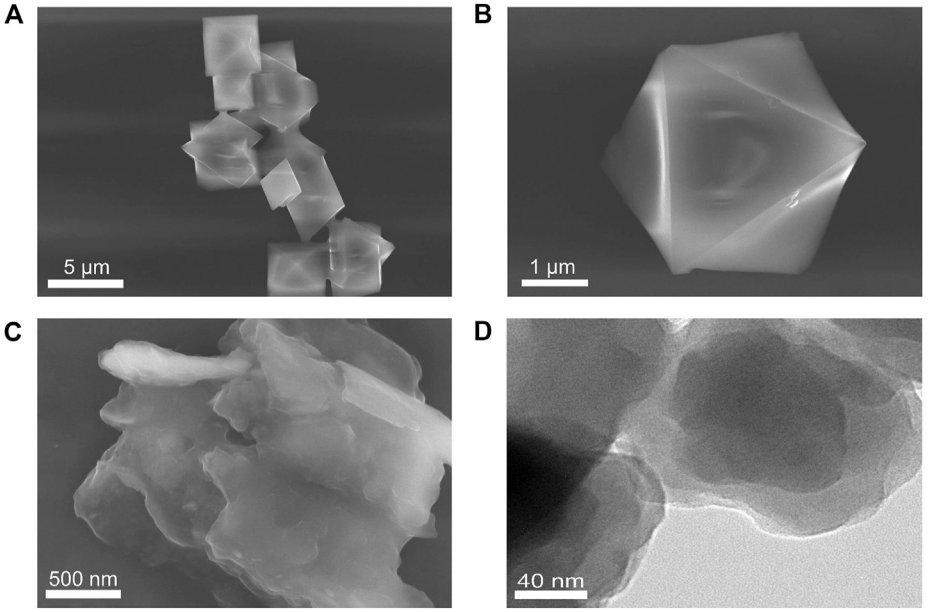

FIGURE 1 | (A) SEM image of HKUST-1. **(B)** A magnified SEM image of HKUST-1. **(C)** SEM image of Cu-TCPP. **(D)** TEM image of Cu–TCPP.

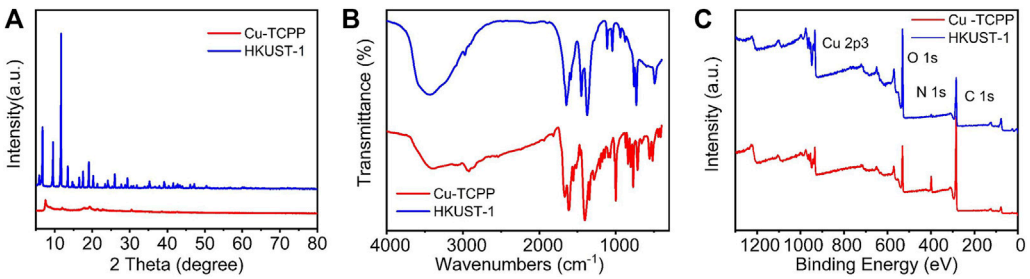

FIGURE 2 | (A) XRD pattern of Cu-TCPP and HKUST-1. **(B)** FT-IR pattern of Cu-TCPP and HKUST-1. **(C)** XPS pattern of Cu-TCPP and HKUST-1.

2D Cu-MOF or 3D Cu-MOF (1 mg/ml) dispersion was coated onto the surface of bare GCE and dried using an infrared lamp. The obtained electrodes are named Cu-TCPP/GCE and HKUST-1/GCE.

RESULT

Morphological, Structural, and Compositional Characterization of HKUST-1 and Cu-TCPP

The morphology, chemical composition, crystal structures, and functional groups of HKUST-1 and Cu-TCPP were characterized by scanning electron microscopy (SEM), transmission electron microscopy (TEM), X-ray photoelectron spectroscopy (XPS), powder X-ray diffraction (XRD), and Fourier transform infrared (FT-IR) spectroscopy. **Figures 1A,B** are the SEM images of HKUST-1. The prepared HKUST-1 displayed a uniform and octahedral structure with the size range of 1–3 μm. **Figures 1C,D** are the SEM image and TEM image of Cu-TCPP, respectively. The obtained Cu-TCPP displayed a two-dimensional and layer-by-layer structure with a wrinkled surface, indicating that the 2D Cu-TCPP nanosheets with an ultrathin structure had a large surface area. The two kinds of Cu-MOFs were consistent with the previously reported one (Wu et al., 2013; Ma and Zheng, 2020). **Supplementary Figures S1A–D** show the powders and solutions of Cu-MOFs.

In order to determine the crystal structures of the prepared Cu-MOFs, X-ray diffraction (XRD) was carried out. It can be seen from **Figures 2A,D** that 2D Cu-MOF exhibited a peak at $2\theta = 20^{\circ}$ which can be indexed as the (002) crystal plane of Cu-TCPP (Ma et al., 2019). The XRD pattern of HKUST-1 exhibits peaks mainly at the range of $2\theta = 5^{\circ}$–20°, corresponding to the previous report, indicating successful synthesis (Wu et al., 2013). It represented a microporous coordination with the cubic crystalline structure.

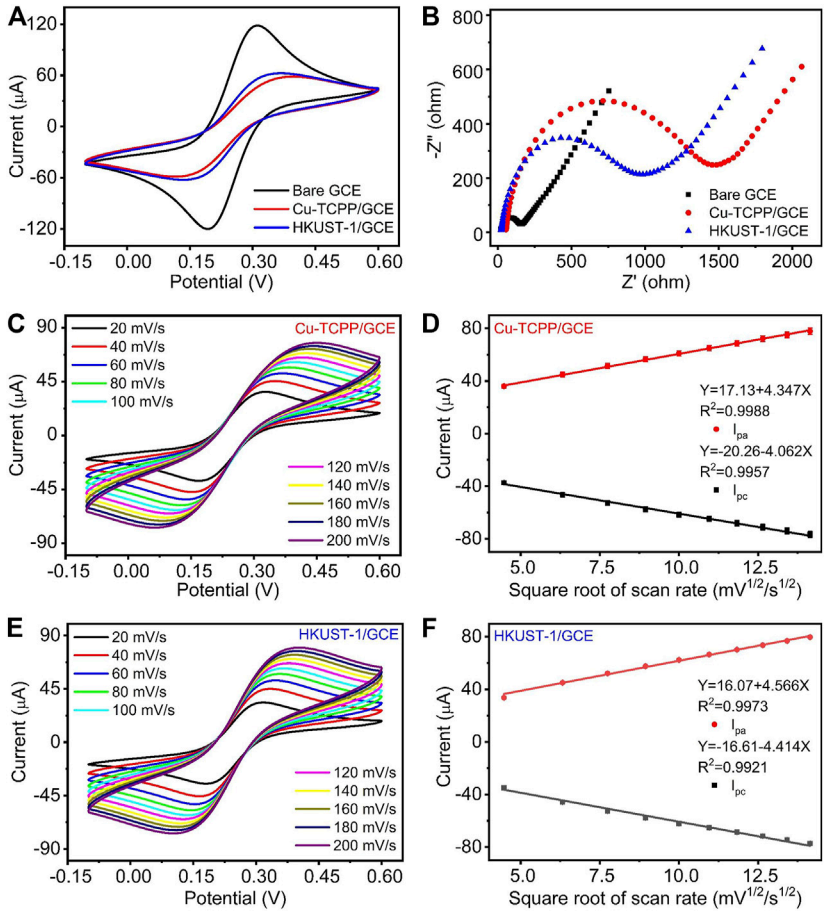

FIGURE 3 | (A, B) CV curves and EIS curves of GCE, Cu-TCPP/GCE, and HKUST-1/GCE. **(C)** CV curves of Cu-TCPP/GCE in the aqueous solution containing 5 mM K_3 [$Fe(CN)_6$]/K_4 [$Fe(CN)_6$] and 0.5 M KCl with different scan rates (20, 40, 60, 80, 100, 120, 140, 160, 180, and 200 mV/s). **(D)** The linear relationships between the electrocatalytic peak current with a square root of the scan rate. **(E)** CV curves obtained by HKUST-1/GCE with different scan rates. **(F)** The linear fitting program of the reduction peak current with a square root of the scan rate obtained by HKUST-1/GCE.

The intense peaks in the XRD demonstrated high crystallinity of the synthesized HKUST-1 samples (Sofi et al., 2019). In addition, the FT-IR spectra were used to identify the functional groups present in the samples. The pattern is shown in **Figure 2B**. The spectra of 2D Cu-MOF and 3D Cu-MOF presented two strong peaks at around 1,400 and 1,620 cm^{-1}, and another strong peak at 3,500 cm^{-1} was contributed by 3D Cu-MOF. The FT-IR spectrum of 3D Cu-MOF demonstrated an almost isobidentate behavior of COO moiety since bands at 1,645, 1,620, 1,570, 1,550, 1,445, and 1,375 cm^{-1} are characteristics of this coordination mode. The latter due to the fact that aniso-bidentate dicopper (II) carboxylate, a type of monomeric clusters, is present in the frameworks (Loera-Serna et al., 2012). Furthermore, the XPS was employed to study the chemical composition and states of Cu-MOFs. The surface characteristics of the synthesized samples were analyzed by XPS. **Figure 2C** demonstrates a full survey of 2D Cu-MOF and 3D Cu-MOF including Cu 2p3, O 1s, N 1s, and C 1s. In the Cu 2p3 region, the HKUST-1 and Cu-TCPP materials show peaks around 900 eV. These results confirmed that two kinds of Cu-MOFs were prepared successfully (Fan et al., 2019).

Electrochemical Performances of Modified Electrodes

To observe the electrochemical performances of bare GCE, Cu-TCPP/GCE, and HKUST-1/GCE, Cyclic voltammetry (CV) and Electrochemical impedance spectroscopy (EIS) were applied to assess their properties. Typically, the EIS plot is composed of a semicircular portion corresponding to the diffusion-limited process and the electron transfer-limited process. The charge transfer resistance (Rct) of the electrode is appropriate to the semicircle diameter. **Figures 3A,B** are the CV pattern and EIS pattern of different modified electrodes, respectively. **Figure 3A** illustrates the CV curve of the bare GCE, Cu-TCPP/GCE, and HKUST-1/GCE. Bare GCE demonstrated the highest redox peak current among three kinds of electrodes in the solution of 5 mM K_3 [$Fe(CN)_6$]/K_4 [$Fe(CN)_6$] containing 0.5 M KCl. After coating 6 μL (1 mg/

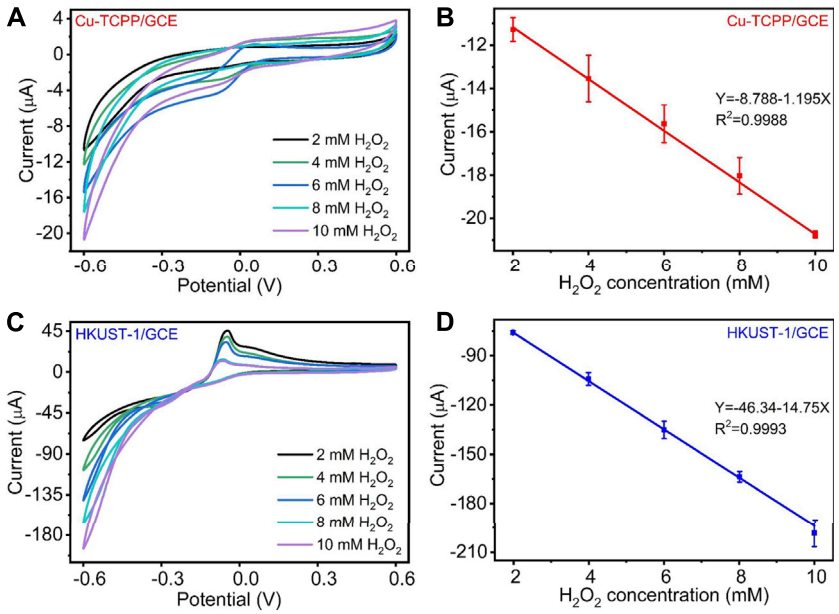

FIGURE 4 | (A) CV curves of Cu-TCPP/GCE for different H_2O_2 concentrations (2, 4, 6, 8, and 10 mM) with a scan rate of 100 mV/s. **(B)** The linear relationships between the electrochemical peak current and H_2O_2 concentration of Cu-TCPP/GCE. **(C)** CV curves of HKUST-1/GCE for different H_2O_2 concentrations (2, 4, 6, 8, and 10 mM). **(D)** The linear relationships between the electrochemical peak current and H_2O_2 concentration of HKUST-1/GCE.

ml) 2D Cu-MOF and 3D Cu-MOF suspension, both the peak current of Cu-TCPP/GCE and HKUST-1/GCE was decreased clearly. The results of EIS measurement matched well with the CV measurement. The EIS diagrams of GCE, Cu-TCPP/GCE, and HKUST-1/GCE are given in **Figure 3B**. The HKUST-1/GCE had better electrochemical behavior than the Cu-TCPP/GCE with a lower resistance than Cu-TCPP. The Rct value of Cu-TCPP/GCE could reach around 1,500 Ω which is 500 Ω more than the HKUST-1/GCE. Compared with 2D Cu-MOFs, 3D Cu-MOFs exhibit unique chemical and physical properties in electrochemical detection. It could be contributed by the 3D Cu-MOF with a porous structure and rapid icon reaction kinetics to make it possible for fast electron transmission. The Cu2-clusters in HKUST-1 are coordinated via carboxylate groups to form a so-called paddle-wheel unit which makes it possible to access the unsaturated metal sites to boost up the performance in electrochemical sensing (Kim et al., 2012; Cortes-Suarez et al., 2019). All these electrochemical results obtained by EIS and CV measurements have proved that the electrodes modifications were successful.

Furthermore, we studied the influences of scan rates on electrochemical performances. At the range of scan rates from 20 to 200 mV/s, two kinds of modified electrodes exhibited a similar tendency. With the increase of scan rates, the redox current increased as shown in **Figures 3C,E**. Two kinds of modified electrodes presented a good linear relationship between the reduction peak current and the square root of scan rates as shown in **Figures 3D,F**. The linear relationship of Cu-TCPP/GCE and HKUST-1/GCE is Y (μA) = -20.26–4.062X ($mV^{1/2}*s^{1/2}$), (R^2 = 0.9957), Y (μA) = -16.61–4.414X ($mV^{1/2}*s^{1/2}$), and (R^2 = 0.9921), respectively. A good linear relationship with the square root of the scan rate indicated fast transfer kinetics and a typical diffusion-controlled electrochemical process.

Electrochemical Property of Different Modified Electrodes Toward H_2O_2

To measure the electrocatalytic activity of the two kinds of different structure Cu-MOFs toward H_2O_2 detection, CV measurements were carried out to study the modified electrodes in 0.1 M N_2 statured PBS solution with or without 10 mM H_2O_2. As shown in **Supplementary Figure S2**, three kinds of electrodes exhibited different current responses to H_2O_2. Whether 10 mM H_2O_2 was present or not, the bare GCE performed no significant response. Both Cu-TCPP/GCE and HKUST-1/GCE showed an obvious current response, indicating that Cu-MOFs had excellent catalytic performance toward H_2O_2 reduction. For comparison, **Supplementary Figures S2B,C** demonstrate the electrocatalytic activity of different structures of Cu-MOFs under the absence and presence of 10 mM H_2O_2. In the 0.1 M N_2 saturated PBS containing 10 mM H_2O_2, the reduction peak current of HKUST-1/GCE could reach nearly 200 μA, which was far beyond the peak current of other two kinds of electrodes. **Supplementary Figure S2D** is the histogram of the reduction peak current of the electrodes modified by different materials in 0.1 M N_2 statured PBS with or without 10 mM H_2O_2.

To further evaluate the Cu-MOF-modified electrodes, we applied a range of concentrations of H_2O_2 in 0.1 M N_2 saturated PBS to measure their electrocatalytic performance as depicted in **Figure 4**. **Figures 4A,C** show the CV curves obtained

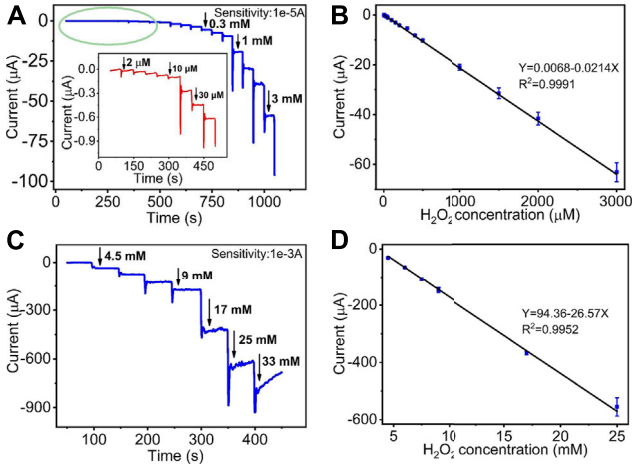

FIGURE 5 | (A) I-t curve of HKUST-1/GCE to the successive addition of low concentration of H_2O_2 in 0.1 M N_2 statured PBS at −0.5 V. The inset shows a magnified image of the I-t curve of low concentration from 2 to 40 μM. **(B)** The linear relationship of the response curve of HKUST-1/GCE with different H_2O_2 concentrations from 2 μM to 3 mM (R^2 = 0.9991). **(C)** Amperometric responses of HKUST-1/GCE to the successive addition of high concentration of H_2O_2 in 100 mM PBS solution. **(D)** The linear fitting program of the reduction peak current of HKUST-1/GCE with different H_2O_2 concentrations from 3 to 25 mM (R^2 = 0.9952).

from H_2O_2 catalysis by the Cu-MOFs. As displayed in **Figures 4A,C**, with the H_2O_2 concentration increased from 2 to 10 mM, the catalytic reduction current obtained by Cu-TCPP/GCE and HKUST-1/GCE increased significantly. It represented that the prepared electrochemical sensors had a good ability for the H_2O_2 electrochemical catalysis. Compared with the peak current of the Cu-TCPP/GCE and HKUST-1/GCE at each H_2O_2 level, HKUST-1/GCE had a better electrochemical performance. Furthermore, Cu-TCPP/GCE and HKUST-1/GCE displayed a great linear relationship between the H_2O_2 concentration and reduction current. The linear equation of Cu-TCPP/GCE was Y (μA) = -8.788–1.195X (mM) (R^2 = 0.9988), and the linearity of HKUST-1/GCE was Y (μA) = -46.34–14.75X (mM) (R^2 = 0.9993) as shown in **Figures 4B,D**, respectively. **Supplementary Figure S3** demonstrates the catalytic reduction currents obtained from two kinds of modified electrodes at different H_2O_2 concentrations.

Amperometric Measurement of H_2O_2

In order to assess the applicability of the HKUST-1/GCE for the electrochemical detection of H_2O_2, amperometric measurement was used to study the response toward H_2O_2 in 0.1 M N_2 saturated PBS. Applied potential will make a great difference to the current response in electrochemical detection. To investigate the optimum potential toward H_2O_2 reduction, I-t curves were obtained by applying different potentials as shown in **Supplementary Figure S4**. With continuous injection of 0.4 mM H_2O_2, the current responses were enhanced with an increasing potential from −0.3 to −0.6 V. Although the HKUST-1/GCE presented the best catalytic activity at the potential of −0.6 V, the background is too high to affect the detection. The potential of −0.3 and -0.4 V could not be selected as the optimal potential because of the low current responses. For these reasons, −0.5 V was chosen as an ideal working potential in the following experiment.

Figures 5A,C display the amperometric current response of the quantitative detection of H_2O_2 on HKUST-1/GCE. Under the sequential injection of different concentration of H_2O_2 to 0.1 M N_2 saturated PBS with stirring at an ideal potential of −0.5 V, the current responses increased clearly. **Figure 5A** shows the amperometric I-T curve at the H_2O_2 concentrations from 2 μM to 3 mM. The insets of **Figure 5A** show the amplified image of the current response at the low concentration from 2 to 40 μM. **Figure 5C** describes the amperometric I-T curve at the H_2O_2 concentrations from 3 to 25 mM. Furthermore, the current responses increased and reached a stable state within 10 s after each step of H_2O_2 injection, indicating the rapid response of HKUST-1/GCE in the electrochemical detection of H_2O_2. **Figures 5B,D** illustrate a great linear relationship between concentrations and the current response. The linear regression equation was Y (μA) = 0.0068–0.0214X (μM) in the H_2O_2 concentrations of 2 μM–3 mM with a correlation coefficient of 0.9991. Good linearity (from 3 to 25 mM) was Y (μA) = 94.36–26.57X (mM) (R^2 = 0.9952). The LOD was found as 0.68 μM with a signal-to-noise ratio of 3. The comparison of the modified electrodes for the detection of H_2O_2 in previous reports is given in **Table 1**. Compared with other research, HKUST-1/GCE exhibited good electrochemical catalysis to H_2O_2 reduction with an extended linear range and a lower LOD. The results could be attributed to the 3D porous structures and fast electron transmission of the materials. All these synergistic factors ensured the excellent electrocatalytic performance of the HKUST-1/GCE.

Selectivity and Stability of HKUST-1/GCE

The selectivity of the sensor represents the ability of real sample detection and practicability. To investigate the catalytic specificity of HKUST-1/GCE further, amperometric measurement was used to study the anti-interference capability of HKUST-1/GCE. At the operating potential of −0.5 V, 1 mM H_2O_2,10 mM potassium chloride (KCl), 10 mM sodium sulfate (Na_2SO_4), 10 mM ascorbic acid (AA), 10 mM citric acid (CA), ethanol absolute, and 1 mM H_2O_2 were injected in 10 ml 0.1 M N_2 statured PBS successively. **Figure 6A** displays the I-T curve obtained by the catalysis of H_2O_2 and some potential interferences. The obvious and rapid current response occurred when the 1 mM H_2O_2 was injected into the PBS. In contrast, no obvious current change could be observed after ten folds of interfering species injection in the same solution. **Figure 6B** displays the current response change of the H_2O_2 and other potential interferences. All these results indicated the HKUST-1/GCE sensor with high selectivity for the electrochemical detection of H_2O_2 in the presence of common interferences.

In addition, we studied the stability of the HKUST-1/GCE electrochemical sensors using CV measurement in the PBS solution containing 10 mM H_2O_2 at the same condition. The results of the stability of the electrochemical sensor are displayed in **Supplementary Figure S5**. The electrochemical current

TABLE 1 | Comparison of different electrochemical platforms for hydrogen peroxide sensing.

Electrodes	Detection potential (V)	Linear range (μM)	LOD (μM)	References
NC@rGO[a]	–0.4 V (vs. Ag/AgCl)	5–20,000	3.3	Li et al. (2018b)
Ag@ZIF-67/GCE[b]	–0.25 V (vs. SCE)	5–275; 775–2,775 4,775–16,775	1.5	Dong et al. (2019)
C-ZIF-67/GCE	–0.35 V (vs. SCE)	2.5–212.5 212.5–1662.5 1662.5–6662.5	0.7	Dong and Zheng, (2020)
HPB/CS/GCE[c]	0.1 V (vs. SCE)	8–1848	2.6	Sheng et al. (2017)
$CuCo_2O_4$	–0.55 V (vs. Ag/AgCl)	10–8900	3.0	Cheng et al. (2020)
Cu-MOF	–0.2 V (vs. Ag/AgCl)	1–900	1.0	Zhang et al. (2015)
IE-MoS_2(3.0)[d]	–0.65 V (vs. Ag/AgCl)	0.23–2,200 2,200–14220	0.2	Shu et al. (2019)
Cu-MOF/ERGO/ITO[e]	–0.3 V (vs. Ag/AgCl)	4–17,334	0.44	Golsheikh et al. (2020)
HKUST-1/GCE	–0.5 V (vs. Ag/AgCl)	2–3000 3000–25,000	0.68	This work

[a]*NC, nitrogen-rich core-shell; rGO, reduced graphene oxide.*
[b]*ZIF, zeolitic imidazolate frameworks.*
[c]*HPB, hollow Prussian blue; CS, chitosan.*
[d]*IE, interlayer-expanded.*
[e]*ERGO, electrochemically reduced graphene oxide; ITO, indium tin oxide.*

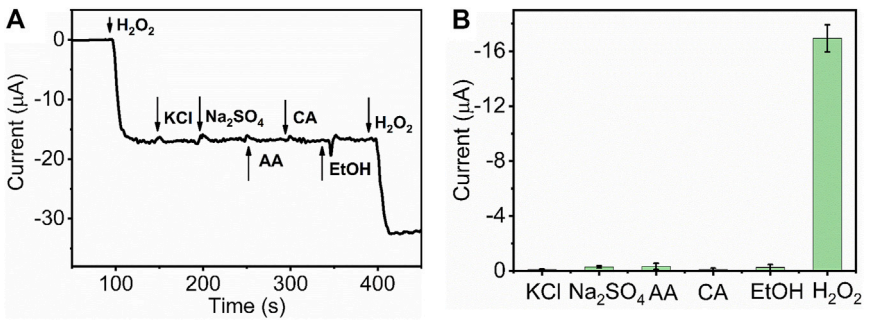

FIGURE 6 | (A) I-t curve of HKUST-1/GCE with the successive injection of 1 mM H_2O_2, 10 mM KCl, 10 mM Na_2SO_4, 10 mM CA, 10 mM AA, C_2H_5OH, and 1 mM H_2O_2 in 0.1 M N_2 statured PBS at an applied potential of –0.5 V. **(B)** Histogram of the current peak obtained by HKUST-1/GCE of H_2O_2 and other potential interferences.

TABLE 2 | Detection of H_2O_2 in the milk sample using HKUST-1/GCE (n = 3).

Sample	Added (μM)	Average founded (μM)	Average recovery (%)	RSD (%)
Milk	40.0	40.1	100.2	4.6
	80.0	77.7	97.1	6.1
	120.0	115.4	96.1	7.7

responses of the sensors retained 90% of their initial value after 5 days. The result of the experiment indicated the good stability of the 3D Cu-MOF-modified electrodes.

Real Sample Analysis of Dairy Products

Generally, H_2O_2 is used as an additive in the food industry for storage, stability, and other purposes. However, over content of H_2O_2 will have a side effect on human beings by causing many diseases. Thus, there is great importance for rapid and specific detection of H_2O_2 in milk samples using a convenient method. Milk samples were purchased from a local supermarket. The practical application of the prepared sensor was carried out to measure the concentration of H_2O_2 in milk samples. The standard addition method and amperometric measurements were used in this experiment section. The milk samples were diluted 20 times using 0.1 M N_2 saturated PBS (pH 7.2). A range of concentrations of H_2O_2 (0, 40, 80, and 120 μM) were added to the milk sample, respectively. Then, milk samples containing different concentrations of H_2O_2 were ready for analysis. The I-T curve obtained by the amperometric measurements was presented in **Supplementary Figure S6**. As shown in

Supplementary Figure S6, no obvious amperometric current response could be seen at the first injection of the diluted milk sample without additional H_2O_2. It proves that the milk sample does not contain endogenous H_2O_2. With the subsequent injection of milk samples containing different concentrations of additional H_2O_2, the current response increased rapidly and obviously, indicating that the sensor is suitable for H_2O_2 detection with good adaptability and practicality in a complex aqueous system. Furthermore, the standard addition method was carried out to calculate the relative standard deviation (RSD) and the recovery rate based on the previous linear regression equation. As shown in **Table 2**, the RSD was less than 8%, and the average recovery rate was 100.2%, 97.1%, and 96.1% (n = 3), respectively. These results demonstrated that the prepared sensor is highly reproducible and effective for H_2O_2 sensing in milk samples.

CONCLUSION

In summary, two kinds of pristine Cu-MOFs with different structures were synthesized successfully for the comparison of morphology and electrocatalytic ability. 3D Cu-MOFs with an octahedral structure performed lower resistance and higher current peak response for the electrochemical catalysis of H_2O_2 than 2D Cu-MOF, demonstrating that the morphology of the Cu-MOFs could influence the electrochemical performance in H_2O_2 reduction. The HKUST-1/GCE presented two wide linear ranges (2 μM–3 mM and 3–25 mM) and a low detection limit of 0.68 μM for H_2O_2 detection in 0.1 M N_2 saturated PBS. Furthermore, the prepared sensor had been applied for the detection of H_2O_2 in milk samples, showing its satisfactory practicability and prospect. This work provided an idea and strategy for the electrochemical detection of H_2O_2. This sensor had great potential for electrochemical detection in the food industry and agricultural system to meet the demand of rapid detection and selectivity in analyses.

DATA AVAILABILITY STATEMENT

The original contributions presented in the study are included in the article/**Supplementary Material**; further inquiries can be directed to the corresponding authors.

AUTHOR CONTRIBUTIONS

This study was conceived and supervised by DS, JP, and TY. Synthesis, structural characterization, and electrochemical measurements were performed by XG, CL, MZ, XuD, and XiD. The analysis of all data were performed by XG and CL. The original draft was written by XG. The manuscript was revised by DS, JP, and TY. All authors contributed to the article and approved the submitted version.

FUNDING

This work was supported by the National Natural Science Foundation of China (82003710), the Natural Science Foundation of Guangdong Province (2020A1515010075), the Project of Educational Commission of Guangdong Province (2018KTSCX108) and the Foundation from Guangdong Traditional Medicine Bureau (20201194).

ACKNOWLEDGMENTS

We thank all members of laboratory for their technical support and academic discussions.

SUPPLEMENTARY MATERIAL

The Supplementary Material for this article can be found online at: https://www.frontiersin.org/articles/10.3389/fchem.2021.743637/full#supplementary-material

REFERENCES

Akyilmaz, E., Oyman, G., Cınar, E., and Odabas, G. (2017). A New Polyaniline-Catalase-Glutaraldehyde-Modified Biosensor for Hydrogen Peroxide Detection. *Prep. Biochem. Biotechnol.* 47 (1), 86–93. doi:10.1080/10826068.2016.1172235

Ammam, M., and Fransaer, J. (2010). Two-enzyme Lactose Biosensor Based on β-galactosidase and Glucose Oxidase Deposited by AC-Electrophoresis: Characteristics and Performance for Lactose Determination in Milk. *Sensors Actuators B: Chem.* 148 (2), 583–589. doi:10.1016/j.snb.2010.05.027

Azad, F. N., Ghaedi, M., Dashtian, K., Hajati, S., and Pezeshkpour, V. (2016). Ultrasonically Assisted Hydrothermal Synthesis of Activated Carbon-HKUST-1-MOF Hybrid for Efficient Simultaneous Ultrasound-Assisted Removal of Ternary Organic Dyes and Antibacterial Investigation: Taguchi Optimization. *Ultrason. Sonochem.* 31, 383–393. doi:10.1016/j.ultsonch.2016.01.024

Bai, W., Li, S., Ma, J., Cao, W., and Zheng, J. (2019). Ultrathin 2D Metal-Organic Framework (Nanosheets and Nanofilms)-Based xD-2D Hybrid Nanostructures as Biomimetic Enzymes and Supercapacitors. *J. Mater. Chem. A.* 7 (15), 9086–9098. doi:10.1039/c9ta00311h

Chen, H., Li, Q.-H., Yan, W., Gu, Z.-G., and Zhang, J. (2020). Templated Synthesis of Cobalt Subnanoclusters Dispersed N/C Nanocages from COFs for Highly-Efficient Oxygen Reduction Reaction. *Chem. Eng. J.* 401, 126149. doi:10.1016/j.cej.2020.126149

Chen, S., Lu, J., You, T., and Sun, D. (2021). Metal-Organic Frameworks for Improving Wound Healing. *Coord. Chem. Rev.* 439, 213929. doi:10.1016/j.ccr.2021.213929

Cheng, D., Wang, T., Zhang, G., Wu, H., and Mei, H. (2020). A Novel Nonenzymatic Electrochemical Sensor Based on Double-Shelled CuCo2O4 Hollow Microspheres for Glucose and H2O2. *J. Alloys Compounds* 819, 153014. doi:10.1016/j.jallcom.2019.153014

Chui, S. S., Lo, S., Charmant, J., Orpen, A., and Williams, I. (1999). A Chemically Functionalizable Nanoporous Material [Cu3(TMA)2(H2O)3]n. *Science* 283 (5405), 1148–1150. doi:10.1126/science.283.5405.1148

Conzuelo, F., Gamella, M., Campuzano, S., Ruiz, M. A., Reviejo, A. J., and Pingarrón, J. M. (2010). An Integrated Amperometric Biosensor for the

Determination of Lactose in Milk and Dairy Products. *J. Agric. Food Chem.* 58 (12), 7141–7148. doi:10.1021/jf101173e

Cortés-Súarez, J., Celis-Arias, V., Beltrán, H. I., Tejeda-Cruz, A., Ibarra, I. A., Romero-Ibarra, J. E., et al. (2019). Synthesis and Characterization of an SWCNT@HKUST-1 Composite: Enhancing the CO2 Adsorption Properties of HKUST-1. *Acs Omega* 4 (3), 5275–5282. doi:10.1021/acsomega.9b00330

Domínguez-Henao, L., Turolla, A., Monticelli, D., and Antonelli, M. (2018). Assessment of a Colorimetric Method for the Measurement of Low Concentrations of Peracetic Acid and Hydrogen Peroxide in Water. *Talanta* 183, 209–215. doi:10.1016/j.talanta.2018.02.078

Dong, L., Yin, L., Tian, G., Wang, Y., Pei, H., Wu, Q., et al. (2020). An Enzyme-free Ultrasensitive Electrochemical Immunosensor for Calprotectin Detection Based on PtNi Nanoparticles Functionalized 2D Cu-Metal Organic Framework Nanosheets. *Sensors Actuators B: Chem.* 308, 127687. doi:10.1016/j.snb.2020.127687

Dong, Y., Duan, C., Sheng, Q., and Zheng, J. (2019). Preparation of Ag@Zeolitic Imidazolate Framework-67 at Room Temperature for Electrochemical Sensing of Hydrogen Peroxide. *Analyst* 144 (2), 521–529. doi:10.1039/c8an01641k

Dong, Y., Yang, L., and Zhang, L. (2017). Simultaneous Electrochemical Detection of Benzimidazole Fungicides Carbendazim and Thiabendazole Using a Novel Nanohybrid Material-Modified Electrode. *J. Agric. Food Chem.* 65 (4), 727–736. doi:10.1021/acs.jafc.6b04675

Dong, Y., and Zheng, J. (2020). Environmentally Friendly Synthesis of Co-based Zeolitic Imidazolate Framework and its Application as H2O2 Sensor. *Chem. Eng. J.* 392, 123690. doi:10.1016/j.cej.2019.123690

Fan, C., Dong, H., Liang, Y., Yang, J., Tang, G., Zhang, W., et al. (2019). Sustainable Synthesis of HKUST-1 and its Composite by Biocompatible Ionic Liquid for Enhancing Visible-Light Photocatalytic Performance. *J. Clean. Prod.* 208, 353–362. doi:10.1016/j.jclepro.2018.10.141

Fu, L.-Q., Chen, X.-Y., Cai, M.-H., Tao, X.-H., Fan, Y.-B., and Mou, X.-Z. (2020). Surface Engineered Metal-Organic Frameworks (MOFs) Based Novel Hybrid Systems for Effective Wound Healing: A Review of Recent Developments. *Front. Bioeng. Biotechnol.* 8, 576348. doi:10.3389/fbioe.2020.576348

Furukawa, H., Cordova, K. E., O'Keeffe, M., and Yaghi, O. M. (2013). The Chemistry and Applications of Metal-Organic Frameworks. *Science* 341 (6149), 1230444. doi:10.1126/science.1230444

Golsheikh, A. M., Yeap, G.-Y., Yam, F. K., and Lim, H. S. (2020). Facile Fabrication and Enhanced Properties of Copper-Based Metal Organic Framework Incorporated with Graphene for Non-enzymatic Detection of Hydrogen Peroxide. *Synth. Met.* 260, 116272. doi:10.1016/j.synthmet.2019.116272

Gu, Z.-Y., Park, J., Raiff, A., Wei, Z., and Zhou, H.-C. (2014). Metal-Organic Frameworks as Biomimetic Catalysts. *Chemcatchem* 6 (1), 67–75. doi:10.1002/cctc.201300493

Guo, X., Cao, Q., Liu, Y., He, T., Liu, J., Huang, S., et al. (2020). Organic Electrochemical Transistor for *In Situ* Detection of H2O2 Released from Adherent Cells and its Application in Evaluating the *In Vitro* Cytotoxicity of Nanomaterial. *Anal. Chem.* 92 (1), 908–915. doi:10.1021/acs.analchem.9b03718

Hartmann, M., Kunz, S., Himsl, D., Tangermann, O., Ernst, S., and Wagener, A. (2008). Adsorptive Separation of Isobutene and Isobutane on Cu3(BTC)2. *Langmuir* 24 (16), 8634–8642. doi:10.1021/la8008656

He, S.-B., Balasubramanian, P., Chen, Z.-W., Zhang, Q., Zhuang, Q.-Q., Peng, H.-P., et al. (2020). Protein-Supported RuO2 Nanoparticles with Improved Catalytic Activity, *In Vitro* Salt Resistance, and Biocompatibility: Colorimetric and Electrochemical Biosensing of Cellular H2O2. *ACS Appl. Mater. Inter.* 12 (13), 14876–14883. doi:10.1021/acsami.0c00778

Hinks, N. J., McKinlay, A. C., Xiao, B., Wheatley, P. S., and Morris, R. E. (2010). Metal Organic Frameworks as NO Delivery Materials for Biological Applications. *Microporous Mesoporous Mater.* 129 (3), 330–334. doi:10.1016/j.micromeso.2009.04.031

Ivanova, A. S., Merkuleva, A. D., Andreev, S. V., and Sakharov, K. A. (2019). Method for Determination of Hydrogen Peroxide in Adulterated Milk Using High Performance Liquid Chromatography. *Food Chem.* 283, 431–436. doi:10.1016/j.foodchem.2019.01.051

Kang, E. J., Campbell, R. E., Bastian, E., and Drake, M. A. (2010). Invited Review: Annatto Usage and Bleaching in Dairy Foods. *J. Dairy Sci.* 93 (9), 3891–3901. doi:10.3168/jds.2010-3190

Karimi, A., Husain, S. W., Hosseini, M., Azar, P. A., and Ganjali, M. R. (2018). Rapid and Sensitive Detection of Hydrogen Peroxide in Milk by Enzyme-free Electrochemiluminescence Sensor Based on a Polypyrrole-Cerium Oxide Nanocomposite. *Sensors Actuators B: Chem.* 271, 90–96. doi:10.1016/j.snb.2018.05.066

Kim, J., Cho, H.-Y., and Ahn, W.-S. (2012). Synthesis and Adsorption/Catalytic Properties of the Metal Organic Framework CuBTC. *Catal. Surv. Asia.* 16 (2), 106–119. doi:10.1007/s10563-012-9135-2

Lee, J., Farha, O. K., Roberts, J., Scheidt, K. A., Nguyen, S. T., and Hupp, J. T. (2009). Metal-Organic Framework Materials as Catalysts. *Chem. Soc. Rev.* 38 (5), 1450–1459. doi:10.1039/b807080f

Li, D., Wang, M., Cheng, N., Xue, X., Wu, L., and Cao, W. (2017a). A Modified FOX-1 Method for Micro-determination of Hydrogen Peroxide in Honey Samples. *Food Chem.* 237, 225–231. doi:10.1016/j.foodchem.2017.05.065

Li, J., Xia, J., Zhang, F., Wang, Z., and Liu, Q. (2018a). An Electrochemical Sensor Based on Copper-Based Metal-Organic Frameworks-Graphene Composites for Determination of Dihydroxybenzene Isomers in Water. *Talanta* 181, 80–86. doi:10.1016/j.talanta.2018.01.002

Li, Y., You, X., and Shi, X. (2017b). Enhanced Chemiluminescence Determination of Hydrogen Peroxide in Milk Sample Using Metal-Organic Framework Fe-MIL-88NH2 as Peroxidase Mimetic. *Food Anal. Methods* 10 (3), 626–633. doi:10.1007/s12161-016-0617-0

Li, Z., Jiang, Y., Wang, Z., Wang, W., Yuan, Y., Wu, X., et al. (2018b). Nitrogen-Rich Core-Shell Structured Particles Consisting of Carbonized Zeolitic Imidazolate Frameworks and Reduced Graphene Oxide for Amperometric Determination of Hydrogen Peroxide. *Microchim. Acta* 185 (11), 501. doi:10.1007/s00604-018-3032-y

Liu, C.-S., Li, J., and Pang, H. (2020). Metal-Organic Framework-Based Materials as an Emerging Platform for Advanced Electrochemical Sensing. *Coord. Chem. Rev.* 410, 213222. doi:10.1016/j.ccr.2020.213222

Loera-Serna, S., Oliver-Tolentino, M. A., de Lourdes López-Núñez, M., Santana-Cruz, A., Guzmán-Vargas, A., Cabrera-Sierra, R., et al. (2012). Electrochemical Behavior of [Cu3(BTC)2] Metal-Organic Framework: The Effect of the Method of Synthesis. *J. Alloys Compounds* 540, 113–120. doi:10.1016/j.jallcom.2012.06.030

Lu, J., Hu, Y., Wang, P., Liu, P., Chen, Z., and Sun, D. (2020). Electrochemical Biosensor Based on Gold Nanoflowers-Encapsulated Magnetic Metal-Organic Framework Nanozymes for Drug Evaluation with *In-Situ* Monitoring of H2O2 Released from H9C2 Cardiac Cells. *Sensors Actuators B: Chemicalactuat. B: chem.* 311, 127909. doi:10.1016/j.snb.2020.127909

Lu, K., Aung, T., Guo, N., Weichselbaum, R., and Lin, W. (2018). Nanoscale Metal-Organic Frameworks for Therapeutic, Imaging, and Sensing Applications. *Adv. Mater.* 30 (37), 1707634. doi:10.1002/adma.201707634

Lu, Q., Zhao, M., Chen, J., Chen, B., Tan, C., Zhang, X., et al. (2016). *In Situ* Synthesis of Metal Sulfide Nanoparticles Based on 2D Metal-Organic Framework Nanosheets. *Small* 12 (34), 4669–4674. doi:10.1002/smll.201600976

Luan, Q., Gan, N., Cao, Y., and Li, T. (2017). Mimicking an Enzyme-Based Colorimetric Aptasensor for Antibiotic Residue Detection in Milk Combining Magnetic Loop-DNA Probes and CHA-Assisted Target Recycling Amplification. *J. Agric. Food Chem.* 65 (28), 5731–5740. doi:10.1021/acs.jafc.7b02139

Luo, Z., Fan, S., Gu, C., Liu, W., Chen, J., Li, B., et al. (2019). Metal-Organic Framework (MOF)-based Nanomaterials for Biomedical Applications. *Cmc* 26 (18), 3341–3369. doi:10.2174/0929867325666180214123500

Ma, J., Bai, W., and Zheng, J. (2019). Non-Enzymatic Electrochemical Hydrogen Peroxide Sensing Using a Nanocomposite Prepared from Silver Nanoparticles and Copper (II)-Porphyrin Derived Metal-Organic Framework Nanosheets. *Microchim. Acta* 186 (7), 482. doi:10.1007/s00604-019-3551-1

Ma, J., Chen, G., Bai, W., and Zheng, J. (2020). Amplified Electrochemical Hydrogen Peroxide Sensing Based on Cu-Porphyrin Metal-Organic Framework Nanofilm and G-Quadruplex-Hemin DNAzyme. *ACS Appl. Mater. Inter.* 12 (52), 58105–58112. doi:10.1021/acsami.0c09254

Ma, J., and Zheng, J. (2020). Voltammetric Determination of Hydrogen Peroxide Using AuCu Nanoparticles Attached on Polypyrrole-Modified 2D Metal-Organic Framework Nanosheets. *Microchim. Acta* 187 (7), 389. doi:10.1007/s00604-020-04355-y

Mariyappan, V., Keerthi, M., and Chen, S.-M. (2021). Highly Selective Electrochemical Sensor Based on Gadolinium Sulfide Rod-Embedded RGO

for the Sensing of Carbofuran. *J. Agric. Food Chem.* 69 (9), 2679–2688. doi:10.1021/acs.jafc.0c07522

Nascimento, C. F., Santos, P. M., Pereira-Filho, E. R., and Rocha, F. R. P. (2017). Recent Advances on Determination of Milk Adulterants. *Food Chem.* 221, 1232–1244. doi:10.1016/j.foodchem.2016.11.034

Pundir, C. S., Deswal, R., and Narwal, V. (2018). Quantitative Analysis of Hydrogen Peroxide with Special Emphasis on Biosensors. *Bioproc. Biosyst Eng* 41 (3), 313–329. doi:10.1007/s00449-017-1878-8

Qi, Y., Ren, S., Che, Y., Ye, J., and Ning, G. (2020). Research Progress of Metal-Organic Frameworks Based Antibacterial Materials. *Acta Chim. Sinica* 78 (7), 613–624. doi:10.6023/a20040126

Sheng, Q., Zhang, D., Shen, Y., and Zheng, J. (2017). Synthesis of Hollow Prussian Blue Cubes as an Electrocatalyst for the Reduction of Hydrogen Peroxide. *Front. Mater. Sci.* 11 (2), 147–154. doi:10.1007/s11706-017-0382-z

Shi, X., Chen, L., Chen, S., and Sun, D. (2021). Electrochemical Aptasensors for the Detection of Hepatocellular Carcinoma-Related Biomarkers. *New J. Chem.* 45, 15158–15169. doi:10.1039/d1nj01042e

Shu, Y., Zhang, W., Cai, H., Yang, Y., Yu, X., and Gao, Q. (2019). Expanding the Interlayers of Molybdenum Disulfide toward the Highly Sensitive Sensing of Hydrogen Peroxide. *Nanoscale* 11 (14), 6644–6653. doi:10.1039/c9nr00333a

Simon-Yarza, T., Mielcarek, A., and Serre, P. C. (2018). Nanoparticles of Metal-Organic Frameworks: On the Road to *In Vivo* Efficacy in Biomedicine. *Adv. Mater.* 30 (37), 1707365. doi:10.1002/adma.201707365

Singh, P., and Gandhi, N. (2015). Milk Preservatives and Adulterants: Processing, Regulatory and Safety Issues. *Food Rev. Int.* 31 (3), 236–261. doi:10.1080/87559129.2014.994818

Sofi, F. A., Bhat, M. A., and Majid, K. (2019). Cu2+-BTC Based Metal-Organic Framework: A Redox Accessible and Redox Stable MOF for Selective and Sensitive Electrochemical Sensing of Acetaminophen and Dopamine. *New J. Chem.* 43 (7), 3119–3127. doi:10.1039/c8nj06224b

Stanković, V., Đurđić, S., Ognjanović, M., Mutić, J., Kalcher, K., and Stanković, D. M. (2020). A Novel Nonenzymatic Hydrogen Peroxide Amperometric Sensor Based on AgNp@GNR Nanocomposites Modified Screen-Printed Carbon Electrode. *J. Electroanalytical Chem.* 876, 114487. doi:10.1016/j.jelechem.2020.114487

Sun, D., Lu, J., Zhong, Y., Yu, Y., Wang, Y., Zhang, B., et al. (2016). Sensitive Electrochemical Aptamer Cytosensor for Highly Specific Detection of Cancer Cells Based on the Hybrid Nanoelectrocatalysts and Enzyme for Signal Amplification. *Biosens. Bioelectron.* 75, 301–307. doi:10.1016/j.bios.2015.08.056

Sun, D., Yang, D., Wei, P., Liu, B., Chen, Z., Zhang, L., et al. (2020). One-Step Electrodeposition of Silver Nanostructures on 2D/3D Metal-Organic Framework ZIF-67: Comparison and Application in Electrochemical Detection of Hydrogen Peroxide. *ACS Appl. Mater. Inter.* 12 (37), 41960–41968. doi:10.1021/acsami.0c11269

Tan, P., Xie, X.-Y., Liu, X.-Q., Pan, T., Gu, C., Chen, P.-F., et al. (2017). Fabrication of Magnetically Responsive HKUST-1/Fe3O4 Composites by Dry Gel Conversion for Deep Desulfurization and Denitrogenation. *J. Hazard. Mater.* 321, 344–352. doi:10.1016/j.jhazmat.2016.09.026

Tang, D., Tang, J., Su, B., and Chen, G. (2010). Ultrasensitive Electrochemical Immunoassay of Staphylococcal Enterotoxin B in Food Using Enzyme-Nanosilica-Doped Carbon Nanotubes for Signal Amplification. *J. Agric. Food Chem.* 58 (20), 10824–10830. doi:10.1021/jf102326m

Upadhyay, N., Goyal, A., Kumar, A., Ghai, D. L., and Singh, R. (2014). Preservation of Milk and Milk Products for Analytical Purposes. *Food Rev. Int.* 30 (3), 203–224. doi:10.1080/87559129.2014.913292

Wang, Y., Zhao, M., Ping, J., Chen, B., Cao, X., Huang, Y., et al. (2016). Bioinspired Design of Ultrathin 2D Bimetallic Metal-Organic-Framework Nanosheets Used as Biomimetic Enzymes. *Adv. Mater.* 28 (21), 4149–4155. doi:10.1002/adma.201600108

Wei, P., Sun, D., Niu, Y., Lu, X., and Zhai, H. (2020). Enzyme-Free Electrochemical Sensor for the Determination of Hydrogen Peroxide Secreted from MCF-7 Breast Cancer Cells Using Calcined Indium Metal-Organic Frameworks as Efficient Catalysts. *Electrochimica Acta* 359, 136962. doi:10.1016/j.electacta.2020.136962

Wu, R., Qian, X., Yu, F., Liu, H., Zhou, K., Wei, J., et al. (2013). MOF-templated Formation of Porous CuO Hollow Octahedra for Lithium-Ion Battery Anode Materials. *J. Mater. Chem. A.* 1 (37), 11126–11129. doi:10.1039/c3ta12621h

Xue, Y., Zheng, S., Xue, H., and Pang, H. (2019). Metal-organic Framework Composites and Their Electrochemical Applications. *J. Mater. Chem. A.* 7 (13), 7301–7327. doi:10.1039/c8ta12178h

Yang, J., Zhao, F., and Zeng, B. (2015). One-Step Synthesis of a Copper-Based Metal-Organic Framework-Graphene Nanocomposite with Enhanced Electrocatalytic Activity. *RSC Adv.* 5 (28), 22060–22065. doi:10.1039/c4ra16950f

Yao, L., Kong, F.-Y., Wang, Z.-X., Li, H.-Y., Zhang, R., Fang, H.-L., et al. (2020). UV-Assisted One-Pot Synthesis of Bimetallic Ag-Pt Decorated Reduced Graphene Oxide for Colorimetric Determination of Hydrogen Peroxide. *Microchim. Acta* 187 (7), 410. doi:10.1007/s00604-020-04350-3

Zeng, J., Ding, X., Chen, L., Jiao, L., Wang, Y., Windle, C. D., et al. (2019). Ultra-Small Dispersed CuxO Nanoparticles on Graphene Fibers for Miniaturized Electrochemical Sensor Applications. *RSC Adv.* 9 (48), 28207–28212. doi:10.1039/c9ra03802g

Zhang, D., Zhang, J., Zhang, R., Shi, H., Guo, Y., Guo, X., et al. (2015). 3D Porous Metal-Organic Framework as an Efficient Electrocatalyst for Nonenzymatic Sensing Application. *Talanta* 144, 1176–1181. doi:10.1016/j.talanta.2015.07.091

Zhang, M., Qiao, R., and Hu, J. (2020). Engineering Metal-Organic Frameworks (MOFs) for Controlled Delivery of Physiological Gaseous Transmitters. *Nanomaterials* 10 (6), 1134. doi:10.3390/nano10061134

Zhang, R., and Chen, W. (2017). Recent Advances in Graphene-Based Nanomaterials for Fabricating Electrochemical Hydrogen Peroxide Sensors. *Biosens. Bioelectron.* 89, 249–268. doi:10.1016/j.bios.2016.01.080

Zhang, Y., Bo, X., Luhana, C., Wang, H., Li, M., and Guo, L. (2013). Facile Synthesis of a Cu-Based MOF Confined in Macroporous Carbon Hybrid Material with Enhanced Electrocatalytic Ability. *Chem. Commun.* 49 (61), 6885–6887. doi:10.1039/c3cc43292k

Zhang, Y., Lv, Q., Chi, K., Li, Q., Fan, H., Cai, B., et al. (2021). Hierarchical Porous Carbon Heterojunction Flake Arrays Derived from Metal Organic Frameworks and Ionic Liquid for H2O2 Electrochemical Detection in Cancer Tissue. *Nano Res.* 14 (5), 1335–1343. doi:10.1007/s12274-020-3176-z

Zhao, M., Huang, Y., Peng, Y., Huang, Z., Ma, Q., and Zhang, H. (2018). Two-Dimensional Metal-Organic Framework Nanosheets: Synthesis and Applications. *Chem. Soc. Rev.* 47 (16), 6267–6295. doi:10.1039/c8cs00268a

Zhao, M., Wang, Y., Ma, Q., Huang, Y., Zhang, X., Ping, J., et al. (2015). Ultrathin 2D Metal-Organic Framework Nanosheets. *Adv. Mater.* 27 (45), 7372–7378. doi:10.1002/adma.201503648

Conflict of Interest: The authors declare that the research was conducted in the absence of any commercial or financial relationships that could be construed as a potential conflict of interest.

Publisher's Note: All claims expressed in this article are solely those of the authors and do not necessarily represent those of their affiliated organizations, or those of the publisher, the editors, and the reviewers. Any product that may be evaluated in this article, or claim that may be made by its manufacturer, is not guaranteed or endorsed by the publisher.

Copyright © 2021 Guo, Lin, Zhang, Duan, Dong, Sun, Pan and You. This is an open-access article distributed under the terms of the Creative Commons Attribution License (CC BY). The use, distribution or reproduction in other forums is permitted, provided the original author(s) and the copyright owner(s) are credited and that the original publication in this journal is cited, in accordance with accepted academic practice. No use, distribution or reproduction is permitted which does not comply with these terms.